NANO LETTERS

Letter

pubs.acs.org/NanoLett

Spectral and Directional Reshaping of Fluorescence in Large Area Self-Assembled Plasmonic−Photonic Crystals

Boyang Ding,*[,†] Calin Hrelescu,[†] Nikita Arnold,[†] Goran Isic,[†,‡] and Thomas A. Klar[†]

[†]Institute of Applied Physics, Johannes Kepler University, 4040 Linz, Austria

[‡]Institute of Physics, University of Belgrade, Pregrevica 118, 11080 Belgrade, Serbia

Supporting Information

ABSTRACT: Spectral and directional reshaping of fluorescence from dye molecules embedded in self-assembled hybrid plasmonic−photonic crystals has been examined. The hybrid crystals comprise two-dimensional hexagonal arrays of dye-doped dielectric nanospheres, capped with silver semishells. Comparing the reshaped fluorescence spectra with measured transmission/reflection spectra and numerical calculations reveals that the spectral and directional reshaping of fluorescence is the result of its coupling to photonic crystal Bloch modes and to void plasmons localized inside the silver caps.

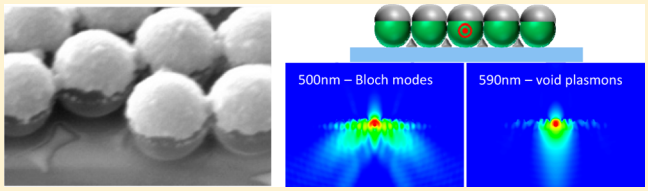

KEYWORDS: *Plasmonic crystal, fluorescence reshaping, localized surface plasmon resonances, Bloch modes, void plasmons, Purcell effect*

An important aim of contemporary nanophotonics is to route and manipulate light by using nanometer length scale structures made of dielectric, metallic or hybrid materials. Such architectures create a structure-defined complex dielectric environment that interacts with electromagnetic waves in various ways, depending on the specific configuration of the nanostructures. For example, light can be localized in a subwavelength volume close to nanometallic objects like noble metal nanoparticles due to the collective oscillations of electrons known as nanoparticle plasmons (sometimes also called localized surface plasmons).[1] Another example is a photonic crystal (PC), which is an architecture with spatially periodic variation of the dielectric permittivity. Light within a certain frequency range cannot propagate in a PC due to the opening of a photonic bandgap.[2−4] When two-dimensional (2D) PCs are made of noble metal, the periodically modulated complex dielectric function of the metallic structures allows for the excitation of surface plasmon polaritons (SPPs) propagating along the metal−dielectric interface[5−7] due to the diffractive coupling into these modes, which is otherwise forbidden for flat films due to wave-vector mismatch between the photons and the SPP. Such structures show distinct dispersive features in their transmission[8] and reflection[9] spectra.

If light emitters, such as quantum dots, dye molecules, or conjugated polymers are placed in the vicinity of metallic nanostructures, fluorescence and the resonant modes of the system start to interact. As a result, the optical properties of light emitters can be influenced in many aspects. For example, the fluorescence lifetime can be manipulated[10] and the emission can be spectrally reshaped[11−15] or spatially redirected.[14−19] Similar ways to manipulate fluorescence have also been shown with dielectric PCs: the lifetime of fluorescence,[3] the spectral shape,[12] and also the direction of emission[12,20] can be altered. Moreover, the optical feedback provided by the dielectric PC[21] or periodic metallic gratings[22,23] may initiate amplified stimulated emission and lasing.

Plasmonic photonic devices can be used in the field of photovoltaics,[24] metamaterials,[25,26] waveguiding,[27] and biosensing,[28] and actually large area structures are necessary for many real life photonic and optoelectronic applications. Unfortunately, up to now many plasmonic structures with precise geometry are mostly fabricated using electron beam or focused ion beam lithography. These techniques, nevertheless, are also characterized by high cost, complicated, and slow manufacturing processes and limited sample area. In order to overcome these shortcomings, nanosphere lithography (NSL) has been used to fabricate large area grating-like plasmonic structures.[29] Specifically, NSL is a lithographic technique using self-assembled opal-based colloidal PCs as templates to produce plasmonic architectures. Plasmonic structures prepared by the NSL approach can be regular arrays of metallic pyramids,[30] spheres,[31] and nanodisks[32] on various substrates. Combined with electrochemical deposition, an array of voidlike nanocavities can be fabricated using hexagonal crystals of nanospheres as sacrificing templates on a gold film.[33] Their optical properties are usually characterized by both, the excitation of nondispersive localized surface plasmon resonances (LSPRs), and traveling SPPs, which can be excited via momentum transfer of a reciprocal lattice vector.[9,34] Because of that, the latter are sometimes also called Bragg plasmons.

In this Letter, we report for the first time the measurement of the transmission, reflection and fluorescence emission spectra

Received: September 20, 2012
Revised: December 20, 2012
Published: January 1, 2013

 © 2013 American Chemical Society

from the same sample. The samples are 2D hexagonal plasmonic-photonic crystals, self-assembled from dye doped polystyrene (PS) spheres on glass substrates, which are optionally capped with plasmonic silver shells (Figure 1 a,b).

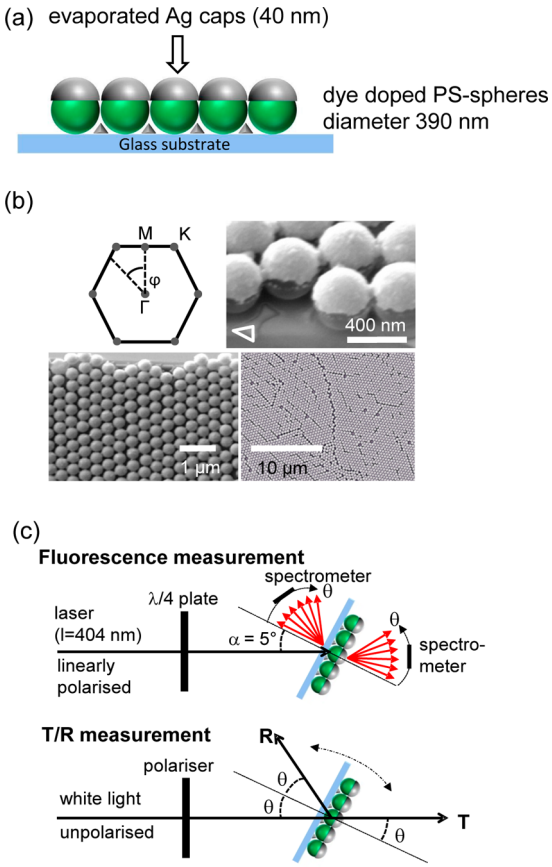

Figure 1. (a) Schematic of the hybrid plasmonic−photonic crystals. (b) Upper left panel: the Brillouin zone of the hexagonal lattice; SEM images of the hexagonally packed monolayer of dye-doped (PS) spheres coated with silver caps viewed from the top (left and right lower panels) and a closer look under 45° (upper right panel). Metal pyramids on the glass substrate are indicated by the white triangle in the upper right panel. (c) Schematics of the experimental setup for angle-resolved fluorescence measurement and transmission/reflection measurements.

Other than in traditional NSL, we do not remove the fluorescing spheres. As a result, we can investigate the spectral and directional reshaping of the fluorescence by the Bloch modes of the PC without silver capping. After the optional evaporation of a semitransparent 40 nm silver layer forming silver caps on the spheres,[35−37] we can study an additional coupling of the fluorescence to the void plasmons inside the caps. In total, our structure forms a hybrid of fluorescing species, and a hexagonal dielectric PC made of PS spheres sustaining distinct Bloch modes.[4,38] The interconnected silver nanocaps support the Bragg modes of traveling surface plasmons as well as LSPRs.[39−41]

Because the substrate is glass and the silver caps are semitransparent, we can study both the reflection and the transmission spectra of the hybrid samples. This allows us to deduce in detail which spectral and directional reshaping of fluorescence is due to a coupling of the fluorescent emission to the PC Bloch modes, to the Bragg plasmons, and to the localized void plasmons inside the silver caps. We find a dispersive coupling of the fluorescence to the PC Bloch modes (which are also present in the samples without silver caps) and a distinct nondispersive coupling to the void plasmons in the Ag caps. However, a coupling of fluorescence to Bragg plasmons seems to be weak in our samples. Previously, it has been shown that the reflection spectra of metal-capped nanosphere PCs differ greatly when collected from the metal coating side or from the substrate side.[42] We now find that also the fluorescence couples to the PC Bloch modes and the LSPR in a very different way, depending on whether the emission takes place into the half space above or below the substrate. Finite difference time domain (FDTD) simulations of the LSPRs in the metallic caps and frequency domain simulations of the Ag-capped PCs (full-fledged periodic structure) support our conclusions.

Previous studies lack the full flexibility to measure fluorescence emission, transmission, and reflection on one and the same sample. Lopez-Garcia et al.[43] reported directional reshaping of fluorescence from dye-doped PCs of PS spheres on a flat gold layer. No metallic caps were applied and the sample was not transparent, so no comparison of the fluorescence and the transmission spectra could be made. Sugawara et al.[44] reported on the strong coupling of void-LSPRs, Bragg plasmons, and molecular excitations on a nontransparent sample. A similar structure was investigated by Jose et al.[45] They observed an enhancement of the excitation of the fluorophores rather than a manipulation of the emission. But again, no transmission spectra could be retrieved because of the use of nontransparent samples.

Our hybrid plasmonic−photonic crystals containing green dye molecules were fabricated by the following procedures (Figure 1a): A hexagonally packed 2D PC of PS spheres loaded with dye molecules (Thermo-Scientific, Waltham, MA, USA, sphere diameter d = 390 nm; dye, "Firefli* Fluorescent Green") was deposited on a glass substrate using self-assembly as reported elsewhere.[46] The extinction and emission spectra of the dye molecules in a PS film and in PS spheres are shown in the Supporting Information (Figure S1). A silver film of 40 nm nominal thickness was evaporated on the freshly crystallized 2D PC. The typical sample size was about 2−4 cm^2. The geometrical parameters (the diameter of the PS spheres and the thickness of the Ag film) are carefully chosen, so that the optical responses of the hexagonal structures can match the emission band of the dyes. The metal film acquires the shape of caps on top of the spheres as shown in Figure 1b. These silver caps are partially connected with each other, forming a 2D periodic array of semishells with a hexagonal lattice. In addition, a small amount of silver was evaporated on the glass substrate through the interstices between the spheres, forming a regular array of silver pyramids. Two reference samples, an unstructured dye-doped PS film (henceforth denoted as unstructured film), and a hexagonally packed monolayer of dye-doped PS spheres without silver coating (henceforth called bare PC) were prepared and compared with the silver coated PC (Ag-capped PC). The unstructured film (thickness ∼3 μm) was made by dissolving the dye-doped PS spheres using toluene, and then spin-coating the dissolved solution on a glass substrate.

The angle-resolved transmission and reflection (T/R) measurement of the samples were performed using a setup previously reported[37,42] (see Figure 1c, lower scheme). Samples were illuminated by white light from a tungsten light source

that is collimated to 1 mm in diameter. The T/R spectra were acquired under s- and p-polarized light, defined as the electric field being perpendicular or parallel to the plane of incidence, respectively. Angle-resolved T/R is measured at distinct angles θ to the sample normal using a spectrometer (B&W TEK, BRC112E-V). θ is varied from 0 to 80° with a step size of 5°. Angle-resolved fluorescence spectra were taken using a similar setup shown in the upper scheme of Figure 1c. A pulsed diode laser (Picoquant, LDH-D-C-405, λ_{exc} = 404 nm, 70 ps pulsewidth) was used to excite the dye molecules from the glass substrate side with a fixed angle of incidence α = 5° to the sample normal. A $\lambda/4$ waveplate is used to convert the linearly polarized laser beam to a circularly polarized one in order to equally excite all the dye molecules with different orientations. The angle-resolved fluorescence into the air side of the samples as well as through the glass substrate side is collected at different angle θ (with respect to the sample normal, as for the T/R measurements). Unless otherwise indicated, a polarization analyzer is placed in front of the spectrometer, in order to pick the s- or p-polarizations of the fluorescence emission.

The fluorescence spectra normal to the surface (θ = 0°, unpolarized) from the unstructured film, the bare PC, and the Ag-capped PC are shown in Figure 2a. In all cases the excitation beam impinges through the glass substrate and the emission normal to the substrate is collected toward the air side. In case of the unstructured film and the bare PC samples, the fluorescence spectra do not depend much on the direction of the fluorescence, that is, whether it is taken toward the air side or through the glass side. Hence, we only show the fluorescence to the air side in case of the unstructured film and the bare PC sample. However, in case of the Ag-capped PC sample, a major difference is observed for these two normal emission directions and hence, spectra for both normal directions are shown (see schemes above the graphs of Figure 2). The fluorescence of the unstructured film exhibits an emission from roughly 450 to 650 nm. The unknown density of dye molecules in the unstructured film makes it impossible to directly compare the fluorescence intensity of the unstructured film with the intensities of the other two samples. However, the fluorescence intensities of the bare PC and the Ag-capped PC can be directly compared. We find that (1) the fluorescence from the Ag-capped PC is much weaker for both directions as compared to the fluorescence from the bare PC and (2) the fluorescence from the Ag-capped PC directed toward the glass side is higher than the fluorescence toward the air side of the sample. The peak-normalized fluorescence spectra of all samples are compared in Figure 2b, where a clear spectral reshaping of the emission from both PC samples (bare PC and Ag-capped PC) can be observed. The peak-normalized fluorescence spectra of the PC samples exhibit specific features at particular vibronic sidebands of the dye molecules, a clear indication of a Purcell type effect. In the case of the Ag-capped PC, this spectral reshaping differs for the two counter-propagating emission directions.

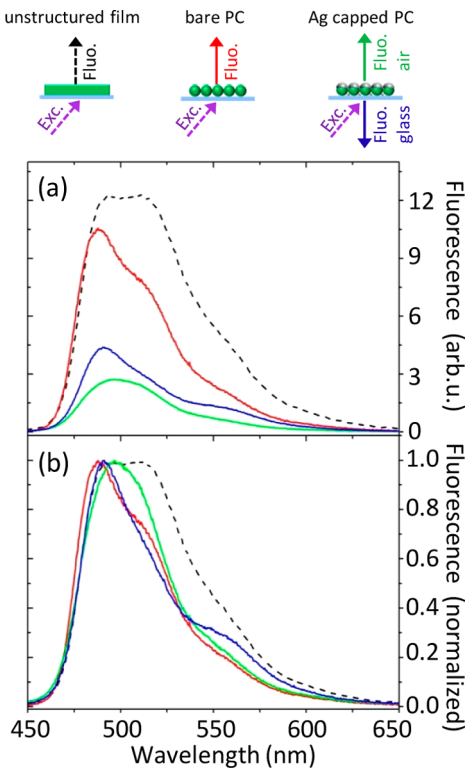

Figure 2. (a) Fluorescence emission of dye molecules measured at θ = 0° (normal to the surface, unpolarized) for samples of an unstructured PS film (black dashed), a bare 2D photonic crystal of dye doped PS spheres without metallic caps (red), and of the Ag-capped photonic crystal into the air side (transmitting the Ag caps) (green) and into the glass substrate side (blue). (b) Normalized fluorescence spectra from (a), same color coding. Schemes above the graph visualize the directions of excitation and detection.

In order to gain insight not only in the spectral reshaping of the fluorescence emission but also in the directional reshaping, we measured the emission as a function of wavelength, angle, and polarization (see Figure 1c for the setup). We denote the fluorescence intensity as $I_{film}(\lambda,\theta)$ in case of the unstructured film, $I_{PC}(\lambda,\theta)$ for the sample of bare PC and $I_{AgPC}(\lambda,\theta)$ for the Ag-capped PC sample. We then normalize the angularly and spectrally resolved fluorescence from the bare PC and from the Ag-capped PC to the fluorescence from the unmodified film and we end up with a quantity that we call the spectral fluorescence reshaping factor F (calculated separately for each polarization)

$$F_{PC}(\lambda, \theta) = \frac{I_{PC}(\lambda, \theta)}{I_{film}(\lambda, \theta)}; \quad F_{AgPC}(\lambda, \theta) = \frac{I_{AgPC}(\lambda, \theta)}{I_{film}(\lambda, \theta)} \tag{1}$$

Figure 3a shows the angular dependence of the experimentally obtained reshaping factors of the fluorescence emission from a bare PC sample to the air side of the sample, F_{air}, for the angular range 0° < θ < 80°, and for s- and p-polarization. It is clearly seen that the fluorescence from the bare PC is dispersively reshaped. Specifically, the fluorescence reshaping factor peaks at λ = 485 nm when θ = 0° for both polarizations. This maximum is rather narrow and it redshifts rapidly with increasing detection angle. The dispersions for s- and p-polarization are slightly different; specifically the p-polarized fluorescence shows the steeper dispersion. The angle-resolved transmission spectra of the bare PC sample are shown in Figure 3d. For each incidence angle θ, the transmission spectrum of the structure is normalized to its respective values at λ = 900 nm (where diffractive effects are almost negligible).[47] This normalization factors out the systematic increase of reflection toward higher θ and enhances the spectral features that are of interest in our studies. It has been reported that the optical transmission of a bare PC at normal incidence exhibits a minimum;[38] it is at the spectral position $\lambda = Dn_{eff}$, where

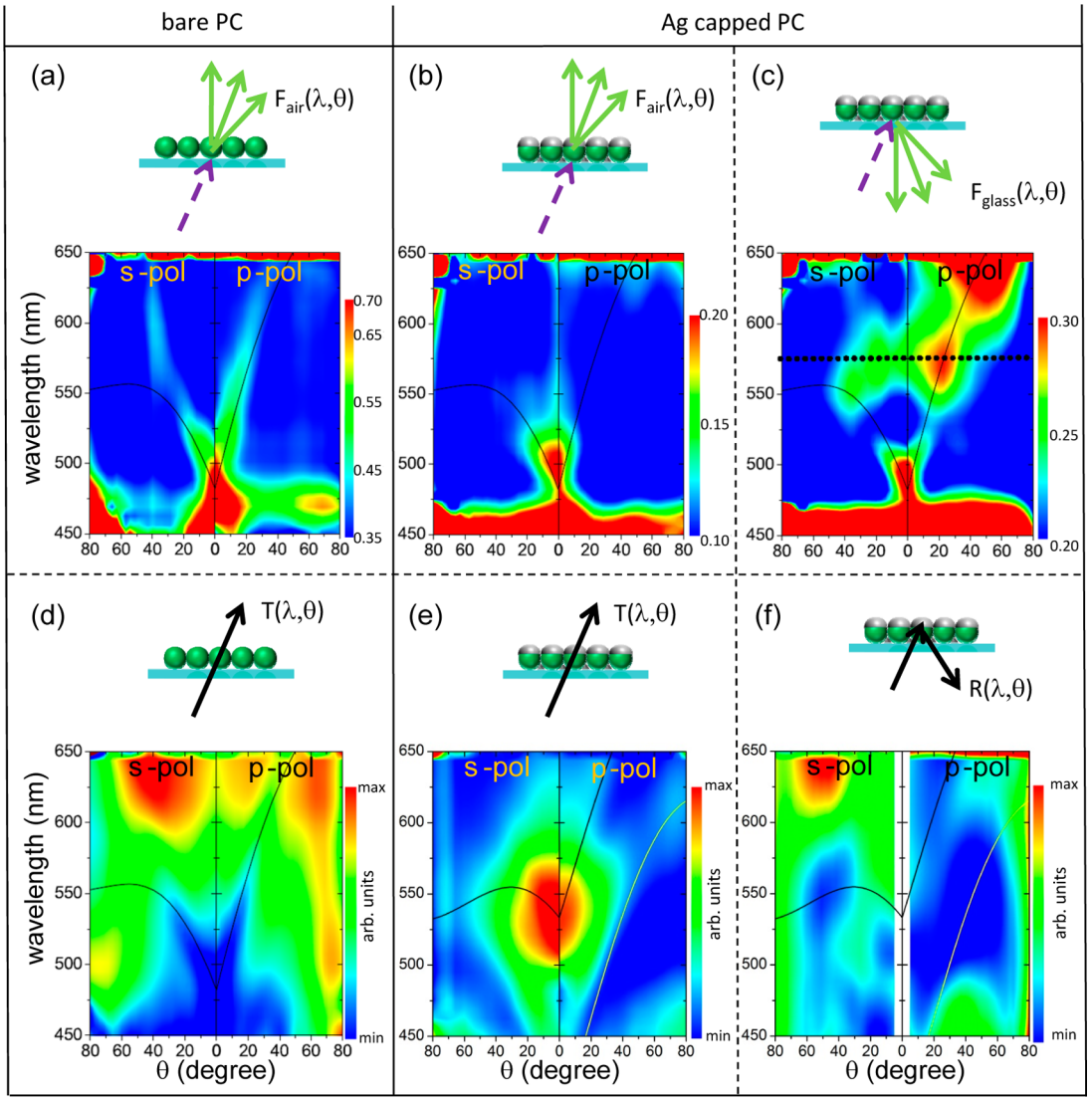

Figure 3. Comparison between the experimental fluorescence and reflection/transmission. Fluorescence reshaping factors for s- and p-polarizations for the bare PC sample (a), for the Ag capped PC sample to the air side (b), and to the glass substrate side (c). The zero-order normalized transmission spectra for s- and p-polarized light of the bare PC (d) and the Ag-capped PC (e) are compared to their counterparts, the fluorescence (a) and (b). The normalized reflection of the Ag-capped PC from the glass side (f) is compared with the fluorescence into the glass side (c). All color-coded intensity plots are experimentally obtained. Black lines in (a–d) are the calculated dispersions of Bloch modes propagating in the PC. Panels (e) and (f) contain the calculated dispersions of plasmonic Bragg modes propagating at the air–silver caps interface (yellow line) and the silver caps–PS spheres interface (black lines). The dotted line in panel (c) indicates the nondispersive feature in fluorescence spectra.

n_{eff} = 1.42 is the effective refractive index of the PC slab (calculated as in the reference[48]), and $D = (\sqrt{3}/2)d$ is the period of the hexagonal lattice (d is the diameter of the sphere). This minimum is due to the coupling into optical eigenmodes or Bloch modes of the 2D PC when the first order diffracted waves propagate in the plane of the PC (similar to Wood anomalies). A minimum of the normalized transmission at θ = 0° is experimentally observed at λ = 485 nm, which agrees well with the calculated result, λ = 479 nm, where D is 338 nm. These in-plane diffraction resonances are angularly dispersive, which can be seen from the dispersive behavior of the minima in the transmission spectra for both polarizations (Figure 3d). Similar to the fluorescence emission (Figure 3a), there is a difference between the dispersions of transmission minima under s- and p-polarized light. This is because when an oblique incident beam illuminates a PC, waves with s- and p-polarizations may preferentially couple into different PC Bloch modes propagating in the plane of the structure. The angular dispersions of the in-plane diffraction resonances can be calculated using the formula[48]

$$\lambda = \frac{\sqrt{3}}{2} d\left(\sqrt{n_{\mathrm{eff}}^2 - \sin^2\theta \sin^2\varphi} - \sin\theta \cos\varphi\right) \tag{2}$$

where φ is the azimuthal angle with respect to the Γ-M direction of the hexagonal lattice (upper left panel of Figure 1b). As our bare PC has macroscopic domains (right lower panel of Figure 1b), all azimuthal angles φ are typically present within the area of the incident beam spot. However, s- and p-polarized waves may preferentially couple to modes of specific azimuthal orientations. The best fit of dispersion using eq 2 results in azimuthal angles φ = 120.5° for s- and φ = 141° for p-polarizations (black lines in Figure 3d). These numbers are guidelines only, as the true position of the maximum is a result of azimuthal averaging of coupling efficiencies, which may even

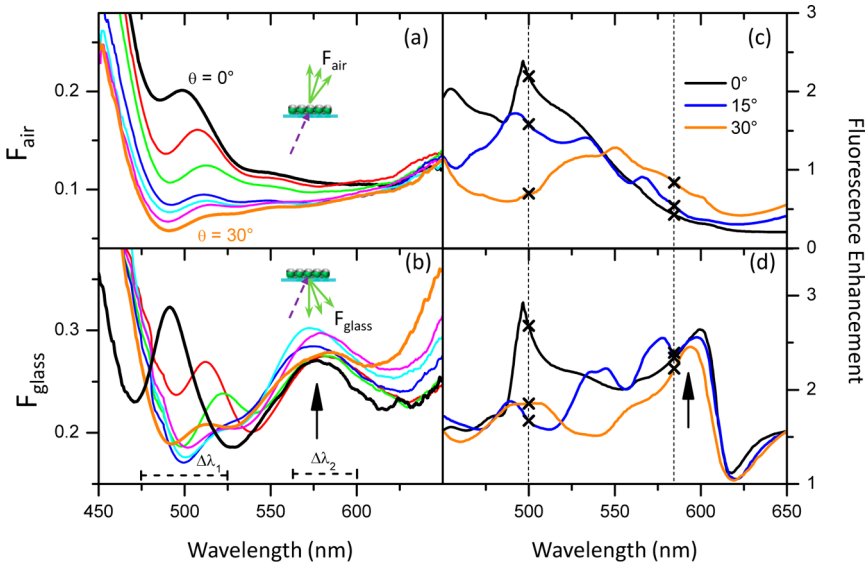

Figure 4. Experimental (a,b) and theoretical (c,d) spectra of the fluorescence reshaping factors. Measured fluorescence of the Ag-capped PC sample for p-polarization in the angular range (0−30°) to the air side (a), and to the glass substrate side (b). The fluorescence enhancement simulated at angles (0, 15, and 30°) for p-polarized emission to the air side (c) and to the glass substrate side (d). See main text for details. The arrows in (b,d) indicate the nondispersive feature, which is absent in (a,c). Vertical dashed lines in (c,d) label the spectral positions of 500 and 585 nm. The corresponding magnitudes of fluorescence enhancement (black crosses) are used in Figure 5, right panels.

change with the angle of incidence θ. The obtained theoretical dispersion curves are also plotted on the map of the fluorescence reshaping factor (black lines in Figure 3a). It is evident that the maxima of the fluorescence reshaping factors follow the dispersion of the in-plane PC modes. This matching strongly suggests that the fluorescence is coupled to the PC Bloch modes.[12,43,49] The mechanism of this coupling can be understood by the increase of the local density of optical states into which the excited dye molecules could decay radiatively.

In the following, we will focus on the discussion about the fluorescence reshaping in the Ag-capped PC sample. As discussed before in the case of the normal direction of emission (Figure 2b), the fluorescence from a Ag-capped PC to the air side is more pronounced around 520 nm but less pronounced at 570 nm as compared with the fluorescence toward the glass substrate. Figure 3b,c shows the angularly resolved spectra of the reshaping factors of fluorescence toward the air side (F_{air}) and to the glass substrate side (F_{glass}), respectively. The maximum of F_{air} is observed at λ = 500 nm for θ = 0°. As opposed to the clearly dispersive behavior of reshaping maxima in a bare PC sample (Figure 3a), the dispersion of F_{air} of the Ag-capped PC sample can only be well resolved from 0 to 10° and completely vanishes beyond θ = 20° (Figure 3b). In contrast, F_{glass} exhibits two pronounced features for both polarizations (Figure 3c): the first one is dispersive, that is, the maximum appears at short wavelength (∼490 nm) for normal emission, and red shifts for larger angles; the second is a nondispersive feature, that is, the maximum is centered at 575 nm and is traceable within an angle range of 0 to 50° (dashed line in Figure 3c). As for a bare PC, the dispersion of the fluorescence from the Ag-capped PC sample exhibits different dispersive behavior for s- and p-polarizations. Both follow the dispersive lines of the bare PC (Figure 3d), which are replotted as black lines in Figure 3 b,c for clarity.

The p-polarized spectra of F_{air} and F_{glass} of fluorescence measured from the Ag-capped PC are shown in Figure 4 (a and b) for 0° < θ < 30°. The dispersive maximum at the interval $\Delta\lambda_1$ (around 500 nm) exists for both directions of fluorescence emission. In contrast, the nondispersive feature (labeled by an arrow at the spectral range $\Delta\lambda_2$) is only observed in the case of fluorescence emitted to the glass side. Numerical simulations reveal similar features. Figure 4c,d shows the simulated fluorescence enhancement for p-polarization at θ = 0, 15, and 30° to the air side and to the glass side of the Ag-capped PC sample, respectively. Numerical fluorescence enhancement is defined as a ratio between the calculated intensity of emission from randomly oriented incoherent dipoles in a Ag-capped PC and the emission of the same dipole ensemble in vacuum. The dipole emission intensity at a specific fluorescence angle θ and an azimuthal angle φ with respect to a hexagonal lattice is calculated using the principle of reciprocity. Details and further discussion can be found in the Supporting Information, section "Modeling of fluorescence intensity". One can see that the fluorescence enhancement is typically larger than 1, especially for the fluorescence to the glass side (Figure 4c,d). The experimental reshaping factors have lower absolute values, mainly because they are normalized to the fluorescence from flat dye doped PS films, which are significantly thicker than the PS-spheres monolayer. Theoretical fluorescence enhancement to the air side at θ = 0° (Figure 4c, black curve) has a maximum around 500 nm, which flattens out and red shifts with increasing θ in reasonable agreement with the experimental findings (Figure 4a). Similarly to the experimental reshaping factors, the fluorescence enhancement into the glass side (Figure 4d) shows an additional maximum at around 590 nm irrespective of the fluorescence angle θ.

As reported before,[42] transmission spectra of Ag-capped PCs are identical no matter from which side the transmitted light is collected, whereas the reflection spectra detected from the metal coated side and from the glass substrate side are completely different. Similar behavior of directionally dependent reflectance has also been reported recently in vertically asymmetrically stacked metamaterials.[50] In our fluorescence experiment, the embedded dye molecules emit light inside the

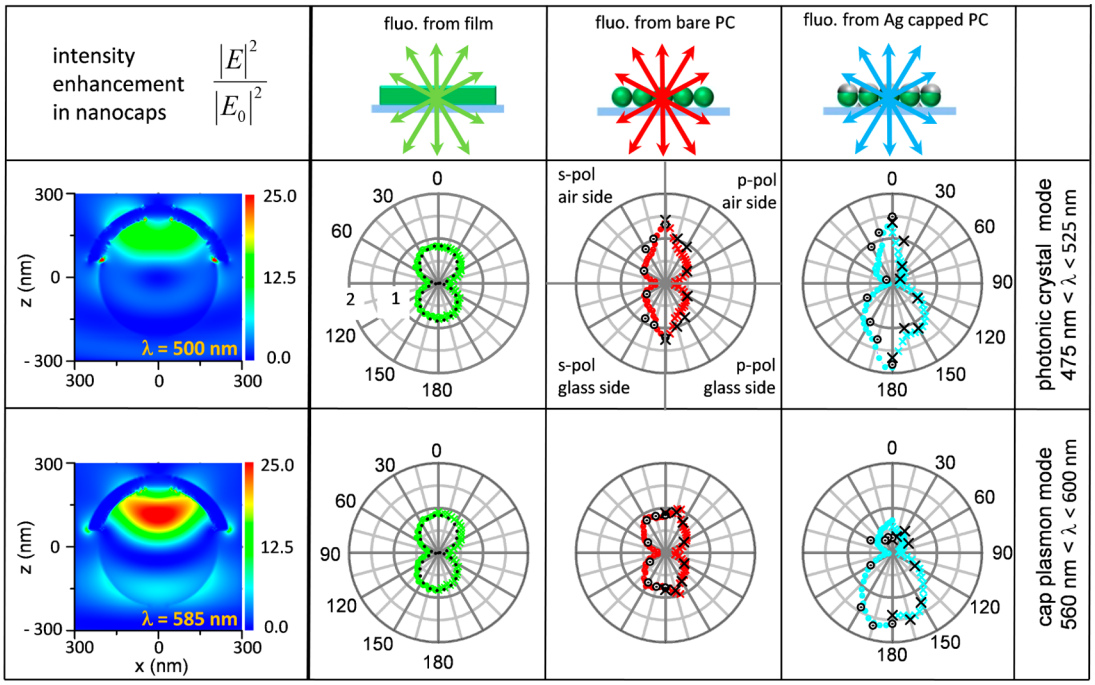

Figure 5. Left column: Calculated intensity enhancement in a single silver coated PS sphere on a glass substrate at the plane of the mid cross-section of the sphere for wavelength 500 nm (upper panel) and 585 nm (lower panel), corresponding to the dispersive (475−525 nm) and nondispersive (560 nm < λ <600 nm) spectral range, respectively. The angular dispersions of the fluorescence intensity, integrated over the corresponding spectral intervals $\Delta\lambda_1$ (475−525 nm) and $\Delta\lambda_2$ (560−600 nm) are shown in the upper and lower lines of polar plots, respectively. The first column of polar plots corresponds to the unstructured (thick) film (green symbols: measured data, black dots: calculated Lambertian emission). The second column corresponds to the plain PC and the third column to the Ag capped PC. As indicated in the upper middle polar plot, each of the plots is organized as follows (clockwise): upper left quadrant, s-polarized fluorescence into the air side; upper right, p-polarized to air side; lower right, p-polarized to glass side; lower left, s-polarized to glass side. In the last two columns of polar plots, black crosses (right half-plane, p-polarization) and dotted circles (left half-plane, s-polarization) correspond to the normalized values of the simulated fluorescence enhancement at 500 nm (upper plots) and 585 nm (lower plots).

concave voids of the silver caps. As a result, the fluorescence collected at the air side of the Ag-capped PC must penetrate through the corrugated silver film, while the fluorescence detected at the glass substrate side interacts with the electromagnetic waves of the mirror dipoles in the Ag layer. The emitted photons in the two antiparallel directions experience different optical paths, and we now want to compare them with the optical path in transmission and reflection upon glass-side illumination (see schematics above Figure 3e,f). Therefore, we compare the features of the reshaping factor of fluorescence toward the air side (Figure 3b) with the transmission spectrum (Figure 3e), and the reshaping factor of fluorescence toward the glass substrate (Figure 3c) with the normalized reflection from the substrate side (Figure 3f). T/R spectra on an extended wavelength range as well as reflection spectra on the air side of the Ag-capped PC can be found in the Supporting Information (Figure S2).

The transmission spectra of the Ag-capped PC exhibit maxima[8,36] at the spectral positions of the Bragg plasmons of the 2D lattice of silver caps, that is, traveling SPP modes that are excited via a reciprocal vector of the hexagonal lattice.[9] There are two sets of Bragg plasmon bands:[37] one is excited at the interface between the spheres and the Ag layer and another is excited at the air−silver interface. The dispersions of these two sets of SPP bands are calculated using eq 2 replacing the n_{eff} with the refractive index of the SPP: $n_{\mathrm{SPP}} = [\varepsilon_{\mathrm{Ag}}\varepsilon_{\mathrm{dielectric}}/(\varepsilon_{\mathrm{Ag}} + \varepsilon_{\mathrm{dielectric}})]^{1/2}$, where $\varepsilon_{\mathrm{Ag}}$ is the permittivity of silver and and $\varepsilon_{\mathrm{dielectric}}$ is the permittivity of the dielectric (either air or an effective medium consisting of PS spheres and air). As shown in Figure 3e, the Bragg plasmon band dominates the transmission spectra of the Ag-capped PC sample. Similar to the case of a bare PC, the dispersion of the Bragg plasmon band on the Ag-capped PC sample is also polarization-dependent (as discussed in more detail in the Supporting Information). In addition, Bragg plasmon bands that appear as dispersive minima can be observed in the reflection spectra of Ag-capped PC (Figure 3f). Surprisingly, we find that the spectral reshaping of fluorescence in the Ag-capped PC (Figures 3b,c) is completely insensitive to the Bragg plasmon modes (Figures 3e,f) but partially relates to the bare PC modes (Figure 3d). Therefore, we replot these modes in Figure 3b,c but not the plasmonic Bragg modes shown in Figure 3e,f. This observation is in contrast to some earlier findings[11,14,15,51] on light emitters in the vicinity of periodic plasmonic structures. However, one should note that in studies where the coupling of fluorescence to Bragg plasmon modes was reported, the plasmonic−photonic crystals have been homogeneously covered with fluorophores. In our case, the dye molecules are confined within each nanosphere, that is, the spatial distribution of dye molecules in the Ag-capped PC sample also obeys a hexagonal pattern. In other words, the majority of the dye molecules are located in the spatial regions where the PC Bloch modes propagate, and only a small fraction is in the immediate vicinity of the Ag−PS−spheres interfaces, where Bragg plasmon modes dominate. As the diameter of our spheres is larger than the typical normal spatial extension of plasmonic modes,[14,15] the coupling of fluorescence to the PC Bloch modes dominates, while coupling to the plasmonic Bragg modes is minor. Coupling of emission from a single dipole into

a bare PC and into a Ag-capped PC is modeled and further discussed in the Supporting Information (Figure S3).

The additional nondispersive maximum in the fluorescence reshaping factor at 575 nm, which is present in the fluorescence into the glass side (Figure 3c) but not into the air side (Figure 3b), suggests some interaction of the fluorescence with a nondispersive localized plasmon. Moreover, the nondispersive maximum can only be seen in the fluorescence through the glass substrate, correlating this feature to the asymmetric configuration of the silver caps. FDTD calculations of the intensity enhancement in a single silver-coated sphere ($|E|^2/|E_0|^2$) (that is the local field intensity normalized by the incident intensity) are shown in the left column of Figure 5 for two different wavelengths, 500 and 585 nm. In this simulation, the normally incident plane wave illuminates the sample from the substrate, mimicking the dye molecules emitting from the void side of the silver cap. At λ = 500 nm, that is, in the spectral range of the dispersive feature ($\Delta\lambda_1$ in Figure 4), the field is only moderately enhanced inside the void. On the contrary, at λ = 585 nm in the spectral position within the nondispersive feature ($\Delta\lambda_2$ in Figure 4) the intensity is strongly enhanced, as a dipole void plasmon resonance is formed inside the silver cap. In both calculations, we assumed an electric-field orientation parallel to the glass plate, that is, we numerically probed the longitudinal void plasmon mode,[34,39,41] sometimes also called the transverse mode in order to distinguish from the axial mode which is in the blue side of the spectrum.[34,39] The cap-shaped plasmonic resonator can facilitate the relaxation of excited dye molecules to specific vibrational ground states if the corresponding transition is in resonance with the LSPR.[13] LSPRs could also be excited on the array of Ag pyramids formed on the substrate of the Ag-capped PC samples. However, according to Haynes et al.[30] and our own numerical calculations (Figure S4 in the Supporting Information), the nanoparticle plasmons related to Ag pyramids have neither spectral nor spatial overlap with the dye molecules confined in the PS spheres. Thus we can conclude that the coupling to the void plasmon is responsible for the nondispersive spectral reshaping of fluorescence in the Ag-capped PC sample, providing a directional decay channel for the excited dye molecules in the void. Summing up, the spectral reshaping of the fluorescence from the Ag-capped PC is the result of a coupling to both the PC modes of the bare PC made of the dielectric PS spheres and the void plasmon modes in metallic semishells. These two couplings reshape the fluorescence at different spectral intervals. However, no pronounced coupling of fluorescence to the Bragg plasmon modes was observed in our hybrid samples.

Finally, we will now examine the polar pattern of fluorescence emission for both spectral intervals, the one which couples to the PC modes and the one which couples to the LSPR of the Ag void plasmons. In the polar plots of Figure 5, we investigate both spectral regions (upper and lower lines of polar plots) for all three samples: the unstructured film (left column of polar plots), the bare PC (central column), and the Ag-capped PC (right column). The angular distribution of the fluorescence intensity for these two bands is calculated using the following formula

$$I(\theta) = \frac{\int_{\lambda_a}^{\lambda_b} I(\lambda, \theta) d\lambda}{\iint I(\lambda, \theta)\sin(\theta) d\lambda\, d\theta} \tag{3}$$

where λ_a and λ_b refer to the starting and end wavelengths of the emission band. In our experiment, the first emission band $\Delta\lambda_1$, from λ_a = 475 to λ_b= 525 nm, corresponds to the dispersive PC modes, while the second band $\Delta\lambda_2$ taken from 560 to 600 nm, corresponds to the localized plasmonic void mode. The fluorescence of the unstructured film exhibits the same directionality as the Lambertian distribution predicts (black dots in the polar plots) for both $\Delta\lambda_1$ or $\Delta\lambda_2$. This good agreement between the calculation and experimental data manifests that the film sample is indeed completely unstructured. With the hexagonally packed bare PC, nanostructuring greatly alters the angular distribution of the fluorescence in the spectral region $\Delta\lambda_1$, where a pronounced forward beaming effect is observed. For the spectral region $\Delta\lambda_2$, the whole emission remains essentially Lambertian even though the influence of the dispersive diffraction resonances can still be seen at particular angles, that is, θ = 20° for p-polarization and θ = 30° for s-polarization (refer to Figure 3a). The fluorescence intensity is uniformly distributed to the air side and to the substrate side. However, when the silver caps are introduced, the directionality of the fluorescence is significantly modified. The modifications are manifold: (1) much less fluorescence goes into the air side passing through the silver caps; (2) in the dispersive band $\Delta\lambda_1$, a pronounced polarization dependence of the directional emission is found; and (3) emission toward the substrate is dominant for the nondispersive band $\Delta\lambda_2$, as the fluorescence is coupled to the void plasmons.

To compare experimental angular emission with theoretical predictions, we can use the simulated fluorescence enhancement spectra (Figure 4). Black crosses in Figure 4c,d indicate the simulated fluorescence enhancement for p-polarization at different angles θ = 0, 15, and 30°. The fluorescence enhancement exhibits various magnitudes at λ = 500 nm (which is representative of the dispersive band $\Delta\lambda_1$) and λ = 585 nm (within the nondispersive band $\Delta\lambda_2$). In order to visually compare the angular variation of simulated fluorescence enhancement with the experimental directionality, we scale the magnitudes of the calculated fluorescence enhancement at all angles, that is, θ = 0, 15, 30, and 60° (not shown in Figure 4) by a common factor, which fits the experimental value to the glass side at θ = 0° exactly. The values at the air side are scaled with the same factor. This is done separately for each polarization and wavelength range. We then add these scaled values as black dotted circles and crosses to the corresponding experimental polar plots in Figure 5. The calculated angular distributions (black symbols) coincide very well with the experimental ones (red and blue symbols). For example, for the Ag-capped PC (the right set of plots), at θ = 15° for p-polarized fluorescence to the glass side (165° on the plots) one can see a slight dip in emission at λ = 500 nm but small maximum for λ = 585 nm. Both of these features are nicely reproduced by the simulations. Only in the case of fluorescence to the air side of a Ag-capped PC at λ = 585 nm, the experimental intensity is higher than the simulated one, probably because the perfectly shaped Ag caps used in the simulations provide a better confinement of the fluorescence toward the glass substrate, while roughness on the air-side of the deposited Ag caps may contribute to the additional scattering of the fluorescence intensity toward the air in the experiments. Taking into account the structure's imperfections, the agreement between the theory and the experiment for the spectra (Figure 4) as well as the directionality (Figure 5) is quite remarkable.

In conclusion, we have designed and fabricated hybrid plasmonic-photonic crystals containing dye molecules by evaporating a metal film on a hexagonally close-packed monolayer of dye-doped nanospheres prepared by colloidal self-assembly. Fluorescence emitted from the dye molecules is reshaped spectrally and directionally both by the coupling of the emission to PC Bloch modes and to the void plasmon modes localized in the silver caps. No coupling of the fluorescence to Bragg plasmon modes has been found. Because of the semitransparency of our sample, the reshaped emission can be detected from both sides of the sample, exhibiting different directionalities in the spectral intervals corresponding to the PC modes and void plasmons, respectively. As a result, the directionality of the fluorescence emitted from the Ag-capped PC is frequency and polarization dependent.

These unique optical properties can be applied in many fields. One possibility would be the design of light-emitting devices that allow tunable directional lighting. For this application, our self-assembled Ag-capped PCs are advantageous over some conventional PC structured LEDs[52,53] for the following reasons: (i) the relatively inexpensive and large-area fabrication process allows for mass-production and (ii) the coexistence of PC Bloch modes and void plasmon modes facilitates the directional sorting of fluorescence. As in our case, these works discuss both spectral and directional reshaping of the emission. However, none of these papers addresses the role of plasmonic modes and their interplay with the emission.

The Ag-capped PCs are also applicable in photovoltaics, e.g., using a process reverse to light emission, the semitransparent structures can be used to enhance light harvesting efficiency in solar cells. Additionally, Ag-capped PCs embedded with high quantum yield fluorophores, in combination with powerful pump lasers can become a good testing ground for plasmonic nanolasers. Here, the desired spectral intervals and preferable lasing modes can be fine-tuned via tailoring the geometrical parameters of the structure.

■ ASSOCIATED CONTENT

Ⓢ Supporting Information

The optical properties of dyes, the T/R spectra, the modeling of fluorescence intensity, and the additional discussion concerning the modeled field distribution. This material is available free of charge via the Internet at http://pubs.acs.org.

■ AUTHOR INFORMATION

Corresponding Author

*E-mail: boyang.ding@jku.at.

Notes

The authors declare no competing financial interest.

■ ACKNOWLEDGMENTS

The authors would like to acknowledge Heidi Piglmayer-Brezina, Alfred Nimmervoll, and Alois Mühlbachler for excellent technical support, and Dr. Klaus Piglmayer for discussions. This work was financially supported by the European Research Council (ERC Starting Grant 257158 "Active NP"). G.I. acknowledges a Postdoctoral Fellowship of the Serbian Ministry of Education and Science.

■ REFERENCES

(1) *Optical Properties of Metal Clusters*; Kreibig, U., Vollmer, M., Springer: Berlin, 1995.
(2) Yablonovitch, E. *Phys. Rev. Lett.* **1987**, *58*, 2059−2062.
(3) Bykov, V. P. *Sov. J. Quant. Electron.* **1975**, *4*, 861−871.
(4) Inoue, M.; Ohtaka, K.; Yanagawa, S. *Phys. Rev. B* **1982**, *25*, 689−699.
(5) Lamprecht, B.; Schider, G.; Lechner, R. T.; Ditlbacher, H.; Krenn, J. R.; Leitner, A.; Aussenegg, F. R. *Phys. Rev. Lett.* **2000**, *84*, 4721−4724.
(6) Haynes, C. L.; McFarland, A. D.; Zhao, L.; Duyne, R. P.; Van; Schatz, G. C.; Gunnarsson, L.; Prikulis, J.; Kasemo, B.; Käll, M. *J. Phys. Chem. B* **2003**, *107*, 7337−7342.
(7) Auguié, B.; Barnes, W. L. *Phys. Rev. Lett.* **2008**, *101*, 143902.
(8) Ebbesen, T. W.; Lezec, H. J.; Ghaemi, H. F.; Thio, T.; Wolf, P. A. *Nature* **1998**, *391*, 667−669.
(9) Kelf, T. A.; Sugawara, Y.; Baumberg, J. J.; Abdelsalam, M.; Bartlett, P. N. *Phys. Rev. Lett.* **2005**, *95*, 116802.
(10) Dulkeith, E.; Morteani, A.; Niedereichholz, T.; Klar, T. A.; Feldmann, J.; Levi, S.; Van Veggel, F.; Reinhoudt, D.; Möller, M.; Gittins, D. *Phys. Rev. Lett.* **2002**, *89*, 12−15.
(11) Bakker, R. M.; Drachev, V. P.; Liu, Z.; Yuan, H.-K.; Pedersen, R. H.; Boltasseva, A.; Chen, J.; Irudayaraj, J.; Kildishev, A. V; Shalaev, V. M. *New J. Phys.* **2008**, *10*, 125022.
(12) Bechger, L.; Lodahl, P.; Vos, W. L. *J. Phys. Chem. B* **2005**, *109*, 9980−9988.
(13) Ringler, M.; Schwemer, A.; Wunderlich, M.; Nichtl, A.; Kürzinger, K.; Klar, T. A.; Feldmann, J. *Phys. Rev. Lett.* **2008**, *100*, 203002.
(14) Vecchi, G.; Giannini, V.; Gómez Rivas, J. *Phys. Rev. Lett.* **2009**, *102*, 146807.
(15) Rodriguez, S. R. K.; Lozano, G.; Verschuuren, M. A.; Gomes, R.; Lambert, K.; De Geyter, B.; Hassinen, A.; Van Thourhout, D.; Hens, Z.; Gómez Rivas, J. *Appl. Phys. Lett.* **2012**, *100*, 111103.
(16) Gersen, H.; García-Parajó, M. F.; Novotny, L.; Veerman, J. A.; Kuipers, L.; Van Hulst, N. F. *Phys. Rev. Lett.* **2000**, *85*, 5312−5315.
(17) Curto, A. G.; Volpe, G.; Taminiau, T. H.; Kreuzer, M. P.; Quidant, R.; Van Hulst, N. F. *Science* **2010**, *329*, 930−933.
(18) Aouani, H.; Mahboub, O.; Bonod, N.; Devaux, E.; Popov, E.; Rigneault, H.; Ebbesen, T. W.; Wenger, J. *Nano Lett.* **2011**, *11*, 637−644.
(19) Aouani, H.; Mahboub, O.; Devaux, E.; Rigneault, H.; Ebbesen, T. W.; Wenger, J. *Nano Lett.* **2011**, *11*, 2400−2406.
(20) Romanov, S. G.; Fokin, A. V.; De La Rue, R. M. *Appl. Phys. Lett.* **1999**, *74*, 1821−1823.
(21) Frolov, S. V.; Vardeny, Z. V.; Zakhidov, A. A.; Baughman, R. H. *Opt. Commun.* **1999**, *162*, 241−246.
(22) Andrew, P.; Turnbull, G. A.; Samuel, I. D. W.; Barnes, W. L. *Appl. Phys. Lett.* **2002**, *81*, 954−956.
(23) Stehr, J.; Crewett, J.; Schindler, F.; Sperling, R.; Von Plessen, G.; Lemmer, U.; Lupton, J. M.; Klar, T. A.; Feldmann, J.; Holleitner, A. W.; Forster, M.; Scherf, U. *Adv. Mater.* **2003**, *15*, 1726−1729.
(24) Atwater, H. A.; Polman, A. *Nat. Mater.* **2010**, *9*, 205−213.
(25) Klar, T. A.; Kildishev, A. V.; Drachev, V. P.; Shalaev, V. M. *IEEE J. Quantum Electron.* **2006**, *12*, 1106−1115.
(26) Xiao, S.; Drachev, V. P.; Kildishev, A. V; Ni, X.; Chettiar, U. K.; Yuan, H.-K.; Shalaev, V. M. *Nature* **2010**, *466*, 735−738.
(27) Kramper, P.; Agio, M.; Soukoulis, C. M.; Birner, A.; Müller, F.; Wehrspohn, R. B.; Gösele, U.; Sandoghdar, V. *Phys. Rev. Lett.* **2004**, *92*, 113903.
(28) Klar, T. A.; Feldmann, J. In *Complex-shaped Metal Nanoparticles. Bottom-Up Synthesis and Applications*; Sau, T. K., Rogach, A. L., Eds.; Wiley-VCH: Weinheim, 2012; pp 395−428.
(29) Fischer, U. C.; Zingsheim, H. P. *J. Vac. Sci. Technol.* **1981**, *19*, 881−885.
(30) Haynes, C. L.; Van Duyne, R. P. *J. Phys. Chem. B* **2001**, *105*, 5599−5611.
(31) Kuznetsov, A. I.; Evlyukhin, A. B.; Gonçalves, M. R.; Reinhardt, C.; Koroleva, A.; Arnedillo, M. L.; Kiyan, R.; Marti, O.; Chichkov, B. N. *ACS Nano* **2011**, *5*, 4843−4849.
(32) Zheng, Y. B.; Juluri, B. K.; Lin Jensen, L.; Ahmed, D.; Lu, M.; Jensen, L.; Huang, T. J. *Adv. Mater.* **2010**, *22*, 3603−3607.

(33) Coyle, S.; Netti, M. C.; Baumberg, J. J.; Ghanem, M. A.; Birkin, P. R.; Bartlett, P. N.; Whittaker, D. M. *Phys. Rev. Lett.* **2001**, *87*, 176801.
(34) Maaroof, A. I.; Cortie, M. B.; Harris, N.; Wieczorek, L. *Small* **2008**, *4*, 2292−2299.
(35) Zhan, P.; Wang, Z.; Dong, H.; Sun, J.; Wu, J.; Wang, H.; Zhu, S. *Adv. Mater.* **2006**, *18*, 1612−1616.
(36) Landström, L.; Brodoceanu, D.; Bäuerle, D.; Garcia-Vidal, F. J.; Rodrigo, S. G.; Martin-Moreno, L. *Opt. Express* **2009**, *17*, 761−772.
(37) Ding, B.; Pemble, M. E.; Korovin, A. V.; Peschel, U.; Romanov, S. G. *Phys. Rev. B* **2010**, *82*, 035119.
(38) Miyazaki, H. T.; Miyazaki, H.; Ohtaka, K.; Sato, T. *J. Appl. Phys.* **2000**, *87*, 7152−7158.
(39) Zhang, Y.; Barhoumi, A.; Lassiter, J. B.; Halas, N. J. *Nano Lett.* **2011**, *11*, 1838−1844.
(40) Cole, R. M.; Baumberg, J. J.; Garcia de Abajo, F. J.; Mahajan, S.; Abdelsalam, M.; Bartlett, P. N. *Nano Lett.* **2007**, *7*, 2094−2100.
(41) King, N. S.; Li, Y.; Ayala-Orozco, C.; Brannan, T.; Nordlander, P.; Halas, N. J. *ACS Nano* **2011**, *5*, 7254−7262.
(42) Ding, B.; Bardosova, M.; Pemble, M. E.; Korovin, A. V.; Peschel, U.; Romanov, S. G. *Adv. Funct. Mater.* **2011**, *21*, 4182−4192.
(43) López-García, M.; Galisteo-López, J. F.; Blanco, A.; Sánchez-Marcos, J.; López, C.; García-Martín, A. *Small* **2010**, *6*, 1757−61.
(44) Sugawara, Y.; Kelf, T. A.; Baumberg, J. J.; Abdelsalam, M. E.; Bartlett, P. N. *Phys. Rev. Lett.* **2006**, *97*, 266808.
(45) Jose, B.; Steffen, R.; Neugebauer, U.; Sheridan, E.; Marthi, R.; Forster, R. J.; Keyes, T. E. *Phys. Chem. Chem. Phys.* **2009**, *11*, 10923−10933.
(46) Moon, G. D.; Lee, T.; Il; Kim, B.; Chae, G.; Kim, J.; Kim, S.; Myoung, J.-M.; Jeong, U. *ACS Nano* **2011**, *5*, 8600−8612.
(47) Nishimura, S.; Abrams, N.; Lewis, B. A.; Halaoui, L. I.; Mallouk, T. E.; Benkstein, K. D.; Van De Lagemaat, J.; Frank, A. J. *J. Am. Chem. Soc.* **2003**, *125*, 6306−6310.
(48) Landström, L.; Arnold, N.; Brodoceanu, D.; Piglmayer, K.; Bäuerle, D. *Appl. Phys. A* **2006**, *83*, 271−275.
(49) Estrada, L. C.; Martinez, O. E.; Brunstein, M.; Bouchoule, S.; Le-Gratiet, L.; Talneau, A.; Sagnes, I.; Monnier, P.; Levenson, J. A.; Yacomotti, A. M. *Opt. Express* **2010**, *18*, 3693−3699.
(50) Kildishev, A. V.; Borneman, J. D.; Ni, X.; Shalaev, V. M.; Drachev, V. P. *Proc. IEEE* **2011**, *99*, 1691−2011.
(51) Livneh, N.; Strauss, A.; Schwarz, I.; Rosenberg, I.; Zimran, A.; Yochelis, S.; Chen, G.; Banin, U.; Paltiel, Y.; Rapaport, R. *Nano Lett.* **2011**, *11*, 1630−1635.
(52) Khokhar, A. Z.; Parsons, K.; Hubbard, G.; Watson, I. M.; Rahman, F.; Macintyre, D. S.; Xiong, C.; Massoubre, D.; Gong, Z.; Gu, E.; Johnson, N. P.; De La Rue, R. M.; Dawson, M. D.; Abbott, S. J.; Charlton, M. D. B.; Tillin, M. *Appl. Opt.* **2011**, *50*, 3233−3239.
(53) Wierer, J. J.; David, A.; Megens, M. M. *Nat. Photonics* **2009**, *3*, 163−169.

Supporting Information

Spectral and Directional Reshaping of Fluorescence in Large Area Self-Assembled Plasmonic-Photonic Crystals

Boyang Ding[1], Calin Hrelescu[1], Nikita Arnold[1], Goran Isic[1,2], and Thomas A. Klar[1]

1. Institute of Applied Physics, Johannes Kepler University, 4040 Linz, Austria

2. Institute of Physics, University of Belgrade, Pregrevica 118, 11080 Belgrade, Serbia

Optical properties of the green dye molecules

The extinction and fluorescent emission spectra of the dye molecules ("Firefli* Fluorescent Green", Thermo Scientific) are shown in Figure S1. The extinction of dyes in polystyrene (PS) nanospheres suspended in water solution (Figure S1a) shows broader tails than the extinction of the same dyes in a PS film (Figure S1b) due to Mie scattering from the spheres at this spectral interval.

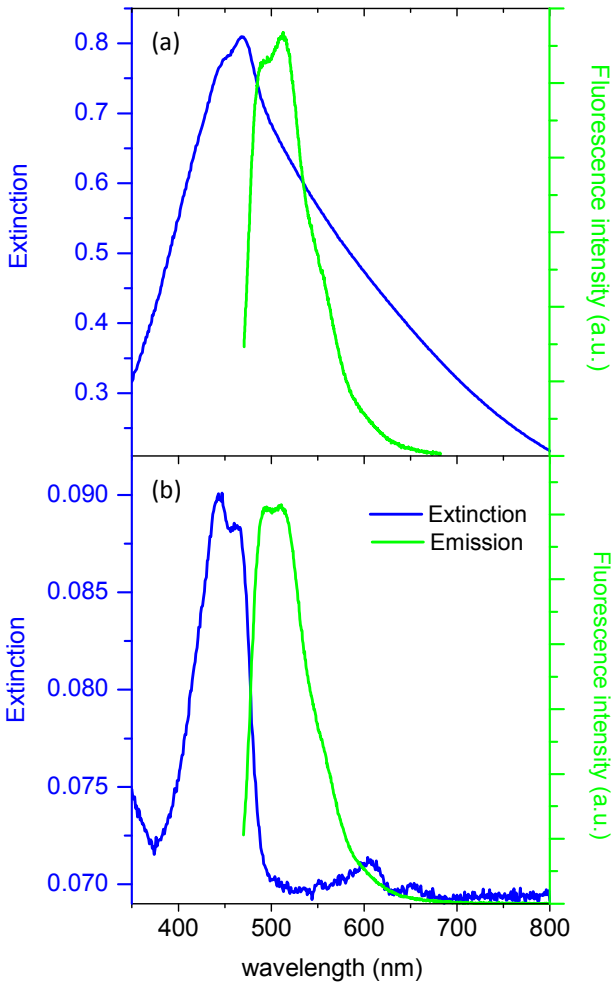

Figure S1. Extinction and fluorescence spectra measured from (a) a water suspension of green dye-doped PS spheres and from (b) a green dye-doped PS film.

Transmission and reflection spectra of the Ag-capped PC sample

Figure S2 shows the normalised transmission and reflection spectra over an extended wavelength range between 450 to 900 nm. The reflection is shown for both directions – into the air and the glass substrate side. The intensity plots are measured data while the black and yellow lines indicate calculated dispersion of the Bragg plasmons.

The dispersion of the main transmission maximum for s-polarisation (Figure S2a, left panel) can be calculated from the Eqn. (2) of the main text, using n_{eff} of the Ag-PC Bragg plasmon and the azimuthal angle $\varphi = 110°$ (black dashed curve). The main transmission maximum for p-polarisation (Fig. S2a, right panel) initially follows the same dispersion curve, but at higher incidence angles ($\theta > 45°$) it crosses over to the Ag-air Bragg plasmon with $\varphi = 154°$ (yellow curve). In addition, the transmission for p-polarisation has a secondary maximum, with a dispersion that can be described by the Ag-PC Bragg plasmon mode with $\varphi = 143°$ (black solid curve). This mode is not observed experimentally for s-polarisation. As in the case of a bare PC, the azimuthal angles are rough guidelines. However two things can be noted here. First, two of the obtained azimuthal angles are close to those used for the transmission of bare PC in Figure 3d. Second, (especially at a larger angle $\theta > 45°$) p-polarised light tends to couple to the Bragg plasmons that propagate more collinearly with the incident wave (φ is closer to 180°). Conversely, s-polarised light preferentially couples into Bragg plasmons with a wavevector almost perpendicular to that of incident wave (φ is closer to 90°). This tendency is natural. Indeed, Bragg plasmons are p-polarised with respect to the plane defined by their propagation direction and the surface normal. At oblique

incidence, roughly speaking, both p- and s-polarised light better couple into those Bragg plasmons, which propagate collinearly with the direction of the dominant component of the electric field. The coupling strength of incident radiation to Bragg plasmons can (in principle) be obtained from the solution of 3D vector Maxwell equations for this complex structure.

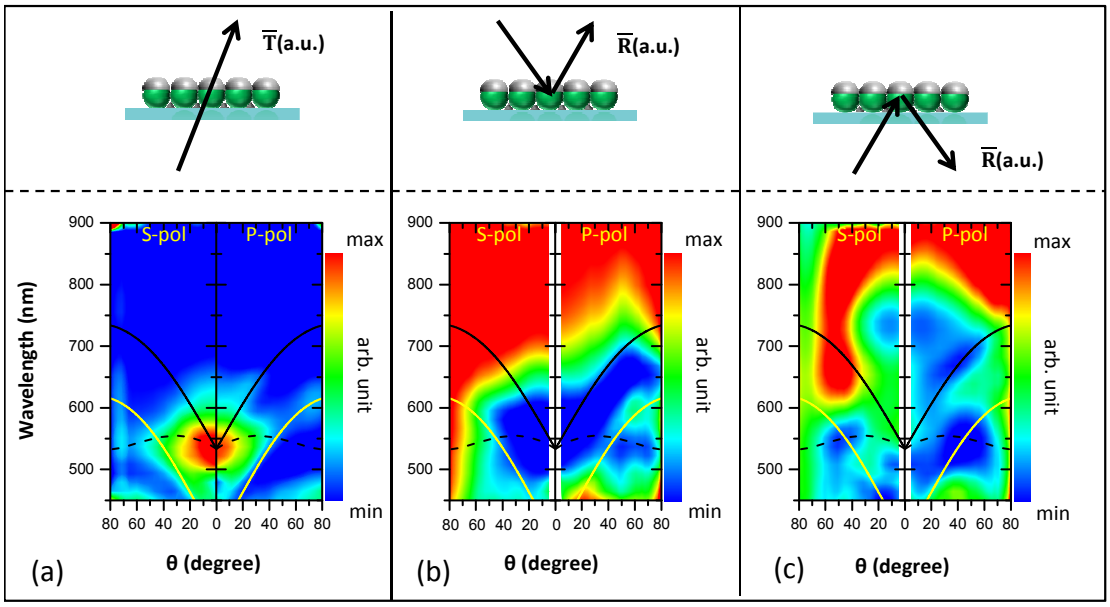

Figure S2. Normalised transmission (a) and reflection spectra collected from the silver side (b) and the glass substrate side (c) of the sample. The calculated dispersions of Bragg plasmon bands at the interface between the PS nanospheres and silver caps with an azimuthal orientation of $\varphi = 143°$ and $\varphi = 110°$ at the hexagonal lattice are plotted with black solid lines and black dashed lines, respectively. The yellow lines indicate the Bragg plasmon bands at the air-silver interface with the azimuthal orientation of $\varphi = 154°$.

Numerical Simulations

For the calculation of the local field distribution, i.e., the field enhancement $|E|/|E_0|$ or the field $|E|$ within the structure, four sets of simulations where performed with two independent programs, but the same modelling parameters: we assume PS-spheres with a radius R_{sphere} = 195 nm and ε_{Ag} = 2.6, Ag-caps with a thickness of h_{cap}(Ag) = 40 nm and use tabulated optical properties from Johnson & Christy[1]. The sharp metallic edges were smoothened with a radius of curvature of 5 nm to avoid singularities.

Single isolated Ag capped PS-spheres (Figure 5 in the main text, left column) and the single dipole emission within the periodic structures (Figure S3) were simulated using Lumerical Solutions, Vancouver, Canada, which uses a Finite Difference Time Domain (FDTD) algorithm. Full-fledged periodic structure upon plane wave (PW) illumination (Figure S4) and the calculated fluorescence enhancement (Figures 4 c,d and numerical data points in the angular diagrams of the Figure 5 from the main text) were modelled with the CST Microwave Studio (Darmstadt, Germany), using a frequency domain solver with adaptive tetrahedral mesh and Floquet boundary conditions.

Modelling of the fluorescence intensity

Figures 4 (c) and (d) in the main text show simulated spectra of fluorescence enhancement, that is the ratio between the fluorescence intensity from dyes in our structure and in vacuum. Such a modelling in different directions and spectral ranges is nontrivial. The density of optical states and the radiative decay rate strongly depend on the dipole position and orientation within the structure.[2] Thus, proper comparison with the experiment should include averaging over positions and orientation of many incoherent dipoles. This is computationally challenging, as individual dipoles break the periodicity of the structure, requiring a large computational domain.

To come around this problem, we adopt the approach based on the reciprocity[3,4] using the software of CST Microwave Studio. More detailed description of this procedure will be reported elsewhere. In short, the argument goes as follows. Due to reciprocity principle, the power $P_\alpha(\Omega)d\Omega$ emitted by the dipole $\mathbf{d}$ into the polarisation α, direction (denoted as Ω) and solid angle $d\Omega$ is related to the local field $\mathbf{E}_\alpha$, which is created at the dipole position by an incident plane wave of the same polarization α coming from the emission direction Ω. The emitted power is a scalar quadratic in d. In a homogeneous space, the dipole emission is p-polarised in dipole-observation plane with $\sin^2\theta$ dependence with respect to dipole axis. In other words, it obeys the following expression:

$$P_\alpha \propto \left|\mathbf{d}\cdot\mathbf{E}_\alpha\right|^2 \qquad \text{(S1)}$$

This expression remains valid when $\mathbf{E}_\alpha$ is the field induced by the incoming plane wave at the dipole position within the structure. Incoherent averaging over the dipole

orientation reduces to $\overline{\cos^2\theta} = 1/3$ and decouples the **d** and $\mathbf{E}_\alpha$ vectors. The average emission becomes $\overline{P}_\alpha(\Omega) \propto d^2 \left|\boldsymbol{\mathcal{E}}_\alpha\right|^2$, where $\boldsymbol{\mathcal{E}}_\alpha = \mathbf{E}_\alpha / E_0$ is the dimensionless vector of field enhancement and E_0 being the amplitude of the incoming plane wave. The emission of homogeneously distributed incoherent dipoles is proportional to the integral of this expression over the volume. It is convenient to normalise it to the fluorescence into direction Ω in the same homogeneous medium (where the enhancement $\left|\boldsymbol{\mathcal{E}}_\alpha\right| = 1$):

$$\frac{\overline{P}_{\alpha,V}(\Omega)}{\overline{P}_{\alpha,V}(\Omega, \left|\boldsymbol{\mathcal{E}}_\alpha\right| = 1)} = \frac{1}{V}\int_V \left|\boldsymbol{\mathcal{E}}_\alpha(\Omega, \mathbf{r})\right|^2 dV \qquad \text{(S2)}$$

The integration includes only the regions where the dyes are present. This approach relates fluorescence intensity to the PW irradiation results. It requires only calculations for one unit cell and includes both orientational and spatial averaging. As a trade-off, multiple PW-irradiation runs are needed to collect the angular emission diagram. The obtained expression assumes homogeneous distribution and excitation of dyes within the volume. Otherwise an excitation factor proportional to the intensity enhancement on the excitation wavelength (and angle of incidence) should be added under the integral in the Equation (S2).[5] Saturation of the excitation may further influence the situation.

Figure 4 (c and d) shows the p-polarised fluorescence enhancement into the angles θ = 0°, 15° and 30°, calculated from the Equation (S2). These angles refer to vacuum values where the fluorescence is registered. Each curve is averaged over three azimuthal angles with respect to the crystal structure, i.e., φ = 0°, 15° and 30° (the influence of φ is in the range of several percent). Figure 4c refers to the fluorescence

to the air side, while Figure 4d refers to the fluorescence to the glass side. The normalisation is to the fluorescence of the same set of incoherent dipoles in homogeneous air. In doing so, we took into account Fresnel reflection losses and change in solid angle at the (thick) glass/air interface (calculated from the Snell's law). In addition, we multiplied the glass-side integral (S2) by $n_{SiO_2} \sim 1.47$, as a dipole in glass emits stronger than a dipole in the air. The change of the homogeneous reference medium (e.g., PS) decreases all fluorescence enhancements by the corresponding refractive index n. Comparison of the absolute numbers with the experiments is complicated by the different amount of dyes and excitation intensities in bare or Ag-capped PC structure and the reference film. For example, strong increase in experimental fluorescence reshaping factors at short wavelengths is an artefact due to the ratio of two small numbers at the rim of the emission spectrum.

Single dipole field distribution in the bare PC and the Ag-capped PC

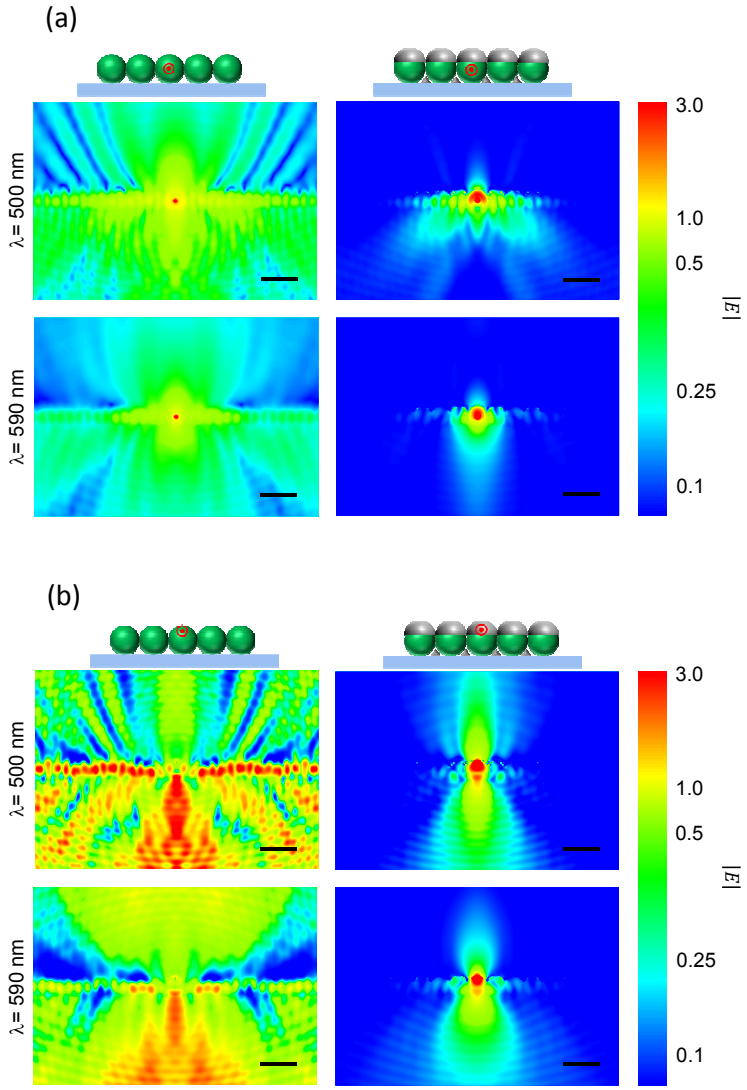

Figure S3. (a) Field distribution $|\mathbf{E}|$ of a single dipole emitter in a bare PC (left panels) and a Ag-capped PC (right panels) at $\lambda = 500$ nm (upper panels) and $\lambda = 590$ nm (lower panels). As shown in the schematics on top, the dipole is positioned at the centre sphere of the PC, along the Γ-M direction of the reciprocal lattice of a hexagonal pattern. Figure (b) illustrates the field distribution $|\mathbf{E}|$ of a single dipole in the same structures as in (a), but with different dipole location, i.e., shifted 150 nm towards the Ag caps. The scale bar in each panel is 1 μm.

In experiments, many dye molecules with various dipole orientations are uniformly distributed within each PS sphere. Such a complex configuration can hardly be modelled by any simulation tool. We therefore calculate the emission pattern of only a single dipole in a bare PC or a Ag-capped PC. By varying the position of the dipole along the film normal, changes in coupling of the dipole radiation to various optical modes within the structures could be revealed. Figure S3 shows the local field $|\mathbf{E}|$ of a single dipole emitter positioned inside the central sphere of a hexagonal array of 23×33 PS spheres (with or without Ag-caps) for two distinct wavelengths $\lambda = 500\,\text{nm}$ and $\lambda = 590\,\text{nm}$, which correspond to the dispersive and the non-dispersive bands $\Delta\lambda_1$ and $\Delta\lambda_2$ labelled in Figure 4. The dipole is oriented along $\Gamma - \text{M}$ direction of the reciprocal lattice and the field $|\mathbf{E}|$ is shown in the plane defined by the $\Gamma - \text{K}$ direction and the film normal. Perfectly matched layers (PMLs) were used on all boundaries of the computational domains simulated with the Lumerical Solutions software.

When the emitter is placed in the centre of the central sphere (Figure S3a), a clear coupling to the PC Bloch modes is observed in all cases, i.e., the electric fields extend horizontally along the array of spheres in both the bare PC and the Ag-capped PC for both $\lambda = 500$ nm and $\lambda = 590$ nm. However, in the Ag-capped PC (right panels of Figure S3a), the fields are confined within several spheres from the emitter, and are mostly localised inside the Ag-capped central sphere. In addition, the directional pattern of the field at the air side is different from that at the glass side. Specifically, in the case of $\lambda = 500$ nm (upper right panel of Figure S3a), the field extending to the air is weaker and is limited to a small solid angle, while the field extending to the

glass side shows two main oblique lobes, resembling the angular pattern of the field for the bare PC (upper left panel of Figure S3a). These features correlate with the directionality diagram shown in the upper right plot of the Figure 5 of the main text. In contrast, the dipole field at the glass side of the Ag-capped PC at $\lambda = 590$ nm (lower right panel of Figure S3a) exhibits a much narrower angular distribution.

Figure S3b shows the field distribution of an off-centre dipole in the central sphere of the bare PC and the Ag-capped PC. In this case, the dipole is positioned at 150 nm above the sphere centre (see the schematics of Figure S3b), i.e., near the field maximum for the void resonance of the silver shell. As in the case of the centred dipole (Figure S3a), electric fields in the Ag-capped PC are mostly confined inside the Ag cap for both wavelengths. However, the field pattern (right panels of Figure S3b) from the Ag-capped PC shows a much better beaming effect to both the air and the glass side, sharply contrasting with the divergent field pattern (left panels of Figure S3b) from the bare PC.

The comparison between Figure S3a and Figure S3b shows that the off-centre dipole position (150 nm above the sphere centre; right panels of Figure S3b) causes better localisation of fields within the Ag-cap void. The light from the centred dipole (right panels of Figure S3a) couples better to the propagating modes of the array of spheres, especially at $\lambda = 500$ nm within the dispersive band $\Delta\lambda_1$. For both dipole positions, only a small fraction of field is distributed near the array of Ag caps. This confirms the experimental findings (Figures 3b,c and Figures 4a,b) that only the coupling of fluorescence to void plasmon modes and to PC Bloch modes is observed,

because the coupling strength to the Bragg plasmons is much weaker in comparison to the coupling to void plasmon and to PC Blcoh modes.

Field distribution in the Ag-capped PC upon PW illumination

The Figure S4 shows the local field enhancement $|E|/|E_0|$ in the structure along the propagation direction and in the cut plane transverse to the propagation direction, at 150 nm from the spheres' centres. This is within the caps, close to the point of maximal intensity of the void plasmon.

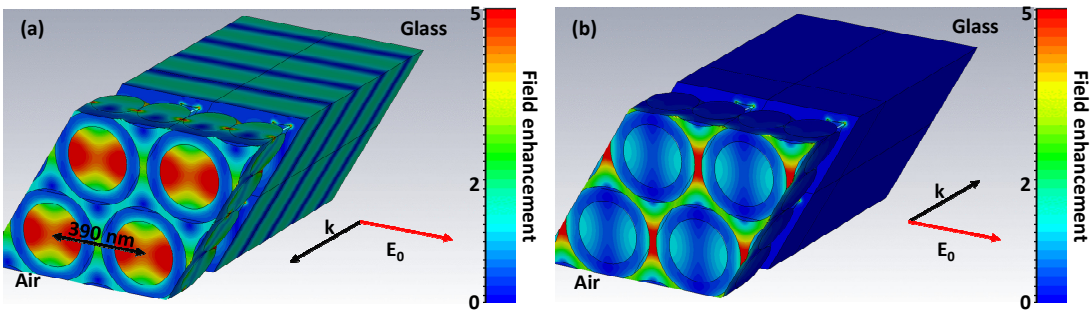

Figure S4. Field enhancement $|E|/|E_0|$ for linearly polarised plane waves (λ = 585 nm, amplitude E_0) normally incident on the periodic Ag-covered PC from the glass side (a), and the air side (b).

Comparison between the Figures S4a and S4b reveals significant enhancement of the electric field inside the PS spheres, when illuminated from the glass side at the 585 nm emission band. This good reciprocal coupling between the light in the spheres and plane waves in the glass elucidates why fluorophores placed inside the capped PS spheres strongly fluoresce into the glass side of the sample. As explained in the main

text, this can be attributed to the excitation of the non-dispersive void plasmon of the silver cap (which exists in the same spectral range) by the incident light. Interestingly, this resonant feature is excited much more prominently upon irradiation from the glass side then upon irradiation from the air side. This happens both for the isolated PS sphere with a single Ag cap (Figure 5, left column), and for the full periodic structure including also the Ag pyramids on the glass support in the interstices between the spheres (Figure S4). Note that hot spots at the tips of the pyramids are spatially well separated from the dye-doped spheres and therefore do not directly influence the reshaping of the fluorescence emission. Further calculations reveal that their resonances typically lie at $\lambda \geq 600$ nm, and are sensitive to the fine details of their geometry.

References

(1) Johnson, P. B.; Christy, R. W. *Phys. Rev. B* **1972**, *6*, 4370–4379.

(2) Novotny, L.Hecht, B. *Principles of Nano-Optics*; 2nd ed.; Cambridge university press: Cambridge, 2012.

(3) Janssen, O. T. A.; Wachters, A. J. H.; Urbach, H. P. *Opt. Express* **2010**, *18*, 24522–24535.

(4) Landau, L. D.; Pitaevskii, L. P.; Lifshitz, E. M. *Electrodynamics of Continuous Media (Volume 8 of A Course of Theoretical Physics)*; 2nd ed.; Elsevier: Amstrdam, 2004.

(5) Ringler, M. Plasmonische Nahfeldresonatorenaus zwei biokonjugierten Goldnanopartikeln (in German), Ludwig-Maximilians-Universität, Munich, Germany, 2008.